# Analysis of statistical quantities in simulation of fluidized beds

Kengo Ichiki* and Hisao Hayakawa†
*Graduate School of Human and Environmental Studies, Kyoto University, Kyoto 606-01, Japan*
(Received 28 April 1997; revised manuscript received 29 August 1997)

Systematic simulations are carried out based on the model of fluidized beds proposed by the present authors [Phys. Rev. E **52**, 658 (1995)]. In our simulation of monolayer particles, the transition of fluidization is a continuous transition. Two types of fluidized phases, the channeling phase and the bubbling phase, are observed. Our simulation suggests that the flow rate plays the role of the effective temperature and the process generating free volume is important for time-averaged statistical quantities. The flow-rate dependence of the diffusion constant suggests the existence of a kind of fluctuation-dissipation relation.
[S1063-651X(98)08902-8]

PACS number(s): 83.70.Hq, 05.60.+w, 03.20.+i, 82.20.Mj

## I. INTRODUCTION

Recently, granular materials have been studied extensively from both experimental and theoretical points of view in the context of the nonequilibrium statistical physics [1–3]. Since the granular materials are dissipative, energy injections are necessary to preserve steady states. Many of the recent studies for granular materials focus on the behavior of systems excited by mechanical activations such as vibration or rotation of vessels. On the other hand, the research on fluidized beds, where systems are excited by the fluid flow, is not as advanced in spite of its variety of dynamical behaviors [4,5].

Fluidized beds have been widely used in chemical industries nearly a hundred years and have been studied from a technological point of view. Fluidized beds consist of granular particles confined in a tall chamber, where fluid is injected from a distributor at the bottom. In experiments, energy injection to the system is controlled by the flow rate of the fluid. For a slow flow rate, the system is in the fixed phase where particles rest on the bottom. When the flow rate exceeds the critical value, particles start moving. Consequently, the system is in the fluidized phase, which contains some phases, for instance, the homogeneous phase, the bubbling phase, and the channeling phase.

There are many models to describe fluidized beds, which can be classified into two categories: two-fluid models and particle-dynamics models. In the two-fluid models, particles are treated as a fluid [5–10]. These models have the benefit of analytical treatments and generalization of their discussion to other systems [11]. However, their basis, such as constitution equations for the particle-phase pressure and the stress tensor, has not been established. On the other hand, the particle-dynamics models describe the direct motion of particles. There are various models such as the distinct element method [12–14]. These models, however, cannot be the basis for the two-fluid models. One of their main problems is that hydrodynamic interactions among particles are oversimplified. For instance, the boundary condition between the particles and fluid is not satisfied on the scale of particles.

Recently, the present authors proposed a numerical model of fluidized beds, where hydrodynamic interaction among particles is calculated with reliable accuracy [15,16]. In this paper we present the results of our systematic simulation for monolayer particles in a fluidized bed and discuss the behaviors of statistical quantities obtained from the simulations.
The content of this paper is as follows. In Sec. II we review the method of our simulation. We show the results in Sec. III, where we observe the transition of fluidization and the existence of two fluidized phases. In Sec. IV we discuss the interpretations of statistical quantities observed in our simulation such as the bed height and the diffusion constant. In Sec. V we summarize our results. In the Appendix we discuss the difficulty of the introduction of particle inertia.

## II. SIMULATION METHOD

In this section we briefly explain our model and how to simulate the dynamics of granular particles in fluid flows. A detailed explanation of our model is given in Refs. [15,16]. For simplicity, we only consider the cases of monodispersed spherical particles. We also neglect the rotational motion of particles. We define the model by the equation of motion for particles

$$\mathrm{St}\frac{d\mathbf{U}}{dt} = -\mathbf{U}+\mathbf{V}+\mathbf{F}_c\,, \tag{2.1}$$

where the boldface letters without superscripts represent vectors in $3N$ dimensions in the $N$-particle system. For example, the velocity of particles $\mathbf{U}$ in Eq. (2.1) has the components

$$\mathbf{U}=\begin{bmatrix}\mathbf{U}^{(1)}\\ \mathbf{U}^{(2)}\\ \vdots\\ \mathbf{U}^{(N)}\end{bmatrix}, \tag{2.2}$$

where the boldface letters with superscripts represent vectors in three dimensions. $\mathbf{F}_c$ in Eq. (2.1) represents hard-core elastic collision among particles and is calculated by the mo-

*Electronic address: ichiki@phys.h.kyoto-u.ac.jp
†Electronic address: hisao@phys.h.kyoto-u.ac.jp

 

mentum exchange for contacting particles. St in Eq. (2.1) is the relaxation time of **U** to the terminal velocity **V** determined by

$$\mathbf{V}-\mathbf{u}^{\infty}=-\vec{R}^{-1}\cdot\mathbf{E}_z, \tag{2.3}$$

where $\mathbf{u}^{\infty}$ is the flow rate of induced fluid, which is equal to the superficial velocity conventionally used for the fluidized beds, and $-\mathbf{E}_z$ is the unit vector directed by gravity. $\vec{R}$ is the resistance matrix representing the hydrodynamic interaction among particles calculated by the method of the Stokesian dynamics [17] with periodic boundary condition [18,19,15]. We also introduce some fixed particles to express the effect of the bottom of the chamber. In this paper we use dimensionless quantities with the aid of the particle radius $a$ and the sedimentation velocity of a single particle in a viscous fluid $U_0=m\tilde{g}/6\pi\mu a$, where $\mu$ is the viscosity of the fluid, $m$ is the mass of particles, and $\tilde{g}=g(\rho_p-\rho_f)/\rho_p$ with the gravitational acceleration $g$ and the densities of the particle $\rho_p$ and the fluid $\rho_f$. Notice that our relaxation model (2.1) is not derived from basic equations because a naive extension of Stokesian dynamics fails to describe collisions among particles (Appendix).

In our simulation, instead of integrating Eq. (2.1), we integrate the ordinary differential equation

$$\mathrm{St}\frac{d\mathbf{u}}{dt}=\exp\left(+\frac{t}{\mathrm{St}}\right)\mathbf{V}, \tag{2.4}$$

where $\mathbf{u}=\mathbf{U}\exp(t/\mathrm{St})$, by the fourth-order Runge-Kutta scheme with fixed time step $\Delta t=0.1$. In each Runge-Kutta loop, we construct the resistance matrix $\vec{R}$ from the positions, calculate the terminal velocity **V**, and then obtain new positions and velocities of particles. After each step $\Delta t$, we pick up the overlapping particles and make them collide by the momentum exchange. To avoid the divergence in the lubrication function for overlapping particles when we calculate $\vec{R}$, we introduce minimum separation $r_c=10^{-17}$. We record positions and velocities of particles every ten steps and calculate the statistical quantities, which will be discussed later.

Equation (2.1) contains two control parameters $u^{\infty}$ and St. For the parameters related to the system size, we choose the number of mobile particles $N_M=256$, the number of fixed particles $N_F=10$, and the size of the unit cell in periodic boundary conditions $(L_x,L_y,L_z)=(34,2,100)$. In this situation, particles are confined in a vertical monolayer, while hydrodynamic interactions are considered in three-dimensional space. We adopt the fixed phase as an initial condition of our simulations, which is constructed from simulations with $u^{\infty}=0$. The choice of the system size and these situations come from the limitation of our computer resources. We have checked that statistical quantities seems to be insensitive to the choice of $L_z$ within the range of $50\leqslant L_z\leqslant 100$ and the choice of the initial conditions is not relevant from the comparison of results with other initial conditions. We have also confirmed that qualitatively similar behaviors are observed in three-dimensional simulations.

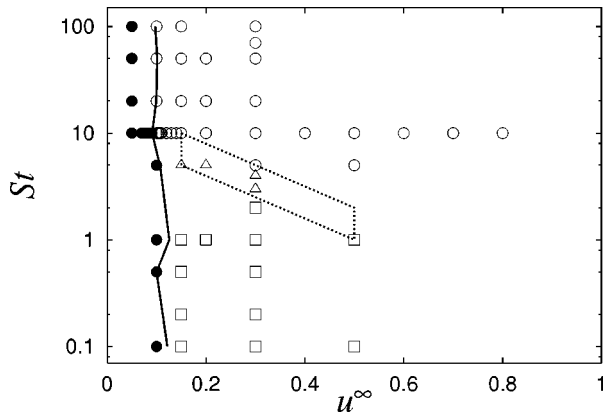


FIG. 1. Plots of points in the parameter space $(u^{\infty},\mathrm{St})$ where we perform a simulation with $N_M=256$, $N_F=10$, and $(L_x,L_y,L_z)=(34,2,100)$. Also shown are the observed phases: fixed phase (●), channeling phase (□), bubbling phase (○), and transition phase (△). We also show the transition line of fluidization $u_c$ with the solid line and the area of the channel-bubble transition with the dotted line, which are discussed in the text.

## III. SIMULATION RESULTS

In this section we present the results of our simulations in detail. We perform simulations at the points plotted in Fig. 1 in parameter space within the range of $0.05\leqslant u^{\infty}\leqslant 0.8$ and $0.1\leqslant \mathrm{St}\leqslant 100$.

In the fixed phase at a slow flow rate, particles are at rest at the bottom. When the flow rate $u^{\infty}$ exceeds the critical flow rate $u_c$, the particles begin to be fluidized. The transition between the fixed phase and the fluidized phase seems to be independent of St. We observe two fluidized phases. One is *the channeling phase* observed for small St, where we can see a channel or a path of fluid flow. Another is *the bubbling phase* observed for large St, where bubbles rise through the particle beds. Their typical time evolution is shown in Figs. 2 and 3. We show the area of channel-bubble transition observed in our simulations as the transition area in Fig. 1.

To characterize the transition of fluidization quantitatively, we calculate the kinetic energy per particle $E(t)$ defined by

$$E(t)=\frac{1}{N_M}\sum_{\alpha=1}^{N_M}[\mathbf{U}^{\alpha}(t)]^2. \tag{3.1}$$

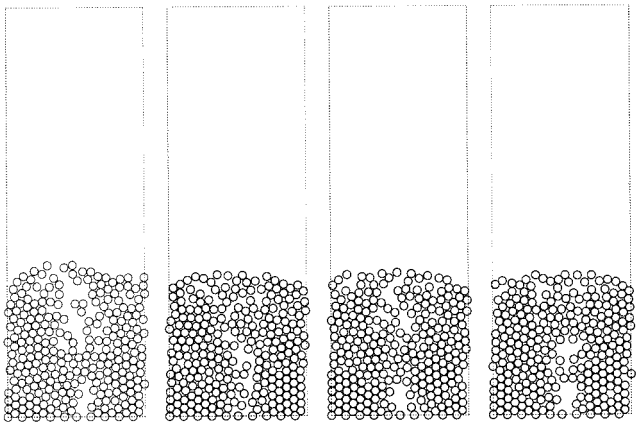

FIG. 2. Typical time evolution of the pattern in the channeling phase at $\mathrm{St}=0.5$ and $u^{\infty}=0.15$. The time proceeds from left to right with an interval of 20 dimensionless units of time.

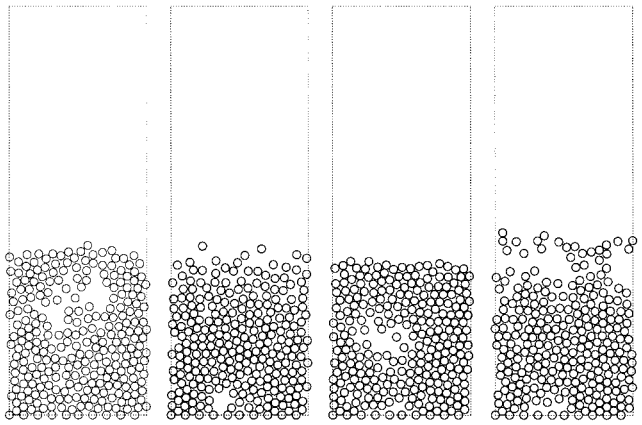

FIG. 3. Typical time evolution of the pattern in the bubbling phase at St=10.0 and $u^{\infty}=0.15$. The time proceeds from left to right with an interval of 20 dimensionless units of time.

A typical behavior of $E(t)$ in the bubbling phase is shown in Fig. 4. We observe a regular behavior after the minimum point following the first peak of $E(t)$. In the channeling phase, we also observe the qualitatively similar behavior of $E(t)$ to Fig. 4, where the period and amplitude of oscillation become smaller. We now introduce the average of $E(t)$ defined by

$$\overline{E}=\frac{1}{\Delta\mathcal{T}}\int_{\Delta\mathcal{T}}dt\ E(t), \tag{3.2}$$

where $\Delta\mathcal{T}$ is the period of the regular behavior in $E(t)$. From Fig. 5 we observe a continuous transition at $u^{\infty}=u_c$, where the data can be well fitted by

$$\overline{E}(u^{\infty})=\begin{cases}0 & (u^{\infty}<u_c)\\ A_E(u^{\infty}-u_c) & (u^{\infty}>u_c).\end{cases} \tag{3.3}$$

The fitting parameters $A_E$ and $u_c$ depend on St. Equation (3.3) defines $u_c$ shown in Fig. 1.

Our results suggest that $u_c$ is independent of St and $\overline{E}(u^{\infty})$ is a linear function of $u^{\infty}$ for any St. It is useful to remember that our model is Galilean invariant, that is, the system with fixed particles of $\mathbf{U}_F=\mathbf{0}$ under the flow rate $u^{\infty}$ is equivalent to that with fixed particles of $\mathbf{U}_F=-u^{\infty}\mathbf{E}_z$ under the flow rate 0. Let us consider how the system is fluidized under the latter situation. First we define $U_{\rm fall}$, which is the falling velocity of the mobile particles in the fixed phase without the support of fixed particles in the frame of $u^{\infty}=0$. If the flow rate $u^{\infty}$ is slower than $U_{\rm fall}$, the mobile particles are supported by the fixed particles moving downward with $u^{\infty}$. Therefore, the system is not fluidized. While the flow rate $u^{\infty}$ is faster than $U_{\rm fall}$, the mobile particles separate from the fixed particles and then the gap between them is generated. The gap may grow into a bubble and propagate upward through the particles or it may construct a channel. Thus the system is fluidized. Our picture means that the critical flow rate $u_c$ is determined by the falling velocity $U_{\rm fall}$, which is independent of St, because $U_{\rm fall}$ is evaluated by the configuration of particles in a fixed phase as the sedimentation rate of suspensions [20] and the configuration is the same for any St. We numerically evaluate $U_{\rm fall}=0.106$ as the average of $\mathbf{V}$ in Eq. (2.3) for the configuration of fixed phase, which is nearly identical to $u_c$.

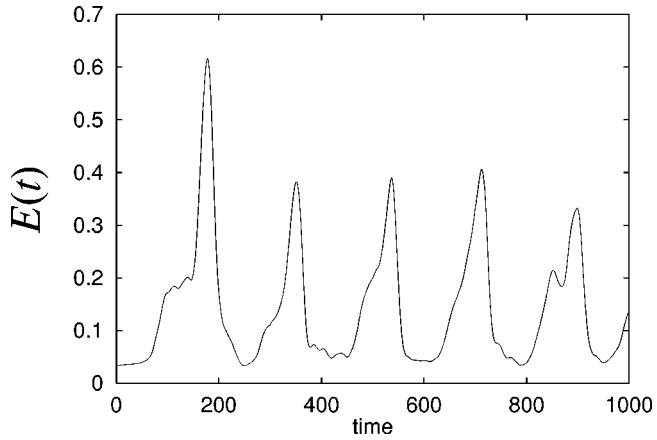


FIG. 4. Typical temporal behavior of $E(t)$ in the fluidized phase. The parameters used here are St=20 and $u^{\infty}=0.3$. The oscillation corresponds to the generation of bubbles.

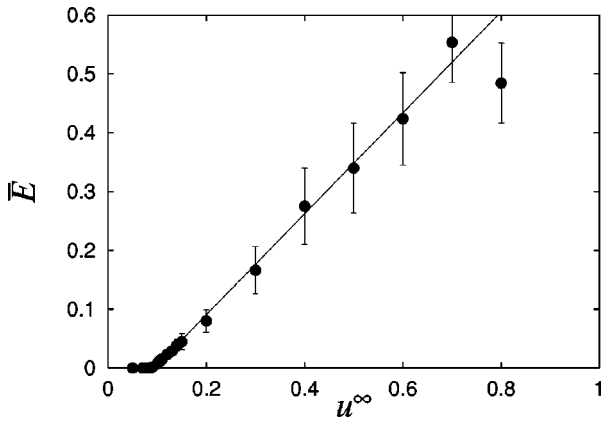


FIG. 5. Flow-rate dependence of the averaged energy $\overline{E}(u^{\infty})$ at St=10. Error bars are their standard deviation. We can see the transition of fluidization at $u^{\infty}=u_c$ and the linear behavior of $\overline{E}$ for the flow rate $u^{\infty}$ in the fluidized phase ($u^{\infty}>u_c$).

The consideration of the Galilean invariant properties also gives us some insight into the linearity of $\overline{E}$ with $u^{\infty}$. In the coordinate with $\mathbf{U}_F=-u^{\infty}\mathbf{E}_z$, it is obvious that the gain of particle energy per unit time from the gravitational potential is proportional to $u^{\infty}$ because the center of mass also falls with the velocity $u^{\infty}$.

Next we discuss the channel-bubble transition. In view of Figs. 2 and 3, it is hard to distinguish the channeling phase from the bubbling phase. At first, we show the variance $V_H$ defined by

$$V_H=\frac{1}{\Delta\mathcal{T}}\int_{\Delta\mathcal{T}}dt[H(t)-\overline{H}]^2, \tag{3.4}$$

where $H$ and $\overline{H}$ are the height of the center of mass and its average defined by

$$H(t)=\frac{1}{N_M}\sum_{\alpha=1}^{N_M}z^{\alpha}(t) \tag{3.5}$$

and

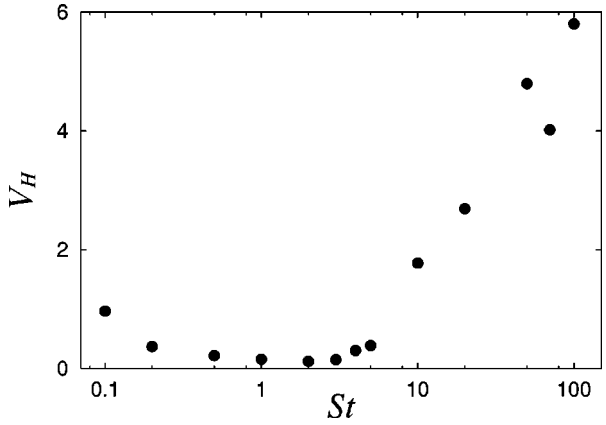


FIG. 6. St dependence of the variance $V_H$ at $u^\infty=0.3$. We can see the transition around St=5. At the channeling phase the variance is small, while at the bubbling phase the variance becomes large.

$$\overline{H}=\frac{1}{\Delta T}\int_{\Delta T} dt\ H(t). \tag{3.6}$$

We expect that $V_H$ is small in the channeling phase and large in the bubbling phase. Figure 6 shows the corresponding behavior for $u^\infty=0.3$ and the transition is observed around St =5. For other cases, the channel-bubble transitions are observed in the area shown in Fig. 1.

We also observe some qualitative changes in the statistical quantities corresponding to the channel-bubble transitions. Figure 7 shows $\overline{E}(\mathrm{St})$ for $u^\infty=0.15$ and 0.3 scaled by the value at St=10 for each case. From this figure we see that $\overline{E}$ increases with St in the channeling phase and $\overline{E}$ decreases with St in the bubbling phase. The behavior in the channeling phase can be understood for the following reason. At St=0, we observe a steady channel and no relative motion among particles. When St increases, the particles on the channel can be fluidized. This means that St is the relaxation time of the particle velocity **U** to their terminal velocity **V**, which is determined under the case of St=0, and the nonrelaxed particles cause the collapse of the channel. Therefore, $\overline{E}(\mathrm{St})$ increases with St in the channeling phase. On the other hand, we observe that $\overline{E}$ decreases with St in the bubbling phase. This may be understood as follows. From Figs. 6 and 7 in the previous paper [15] or in Fig. 4 herein, we have seen that the kinetic energy is generated by bubbles with convective motion of particles. This is because the local difference of the volume fraction of particles causes the relative motion of particles through hydrodynamic interaction. As St increases, trajectories of particles become ballistic and the difference of volume fraction tends to be leveled, since St represents particle inertia. Thus the convective motion caused by bubbles becomes small when St becomes large. In fact, we see a clear bubble and the definite convective motion of particles for St=10 (Fig. 8), while we see a relatively obscure bubble and the weaker convection for St=100 (Fig. 9). Therefore, $\overline{E}(\mathrm{St})$ in the bubbling phase decreases with St. Taking into account the increase of $\overline{E}(\mathrm{St})$ in the channeling phase as a function of St, $\overline{E}(\mathrm{St})$ has a peak around the transition point.

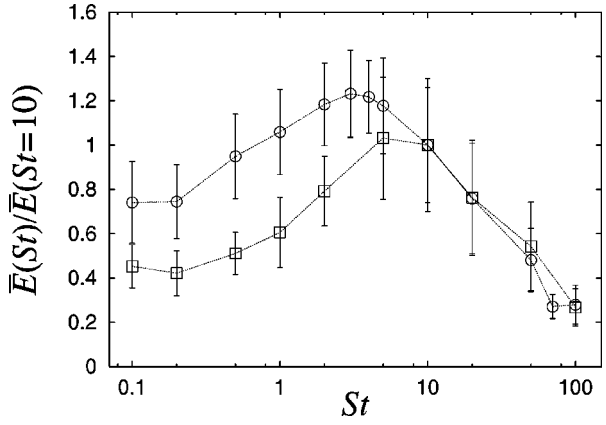


FIG. 7. St dependence of the averaged energy $\overline{E}$ scaled by $\overline{E}(\mathrm{St}=10)$ for $u^\infty=0.15$ (□) and 0.3 (○). For each case we can observe a peak around the channel-bubble transition.

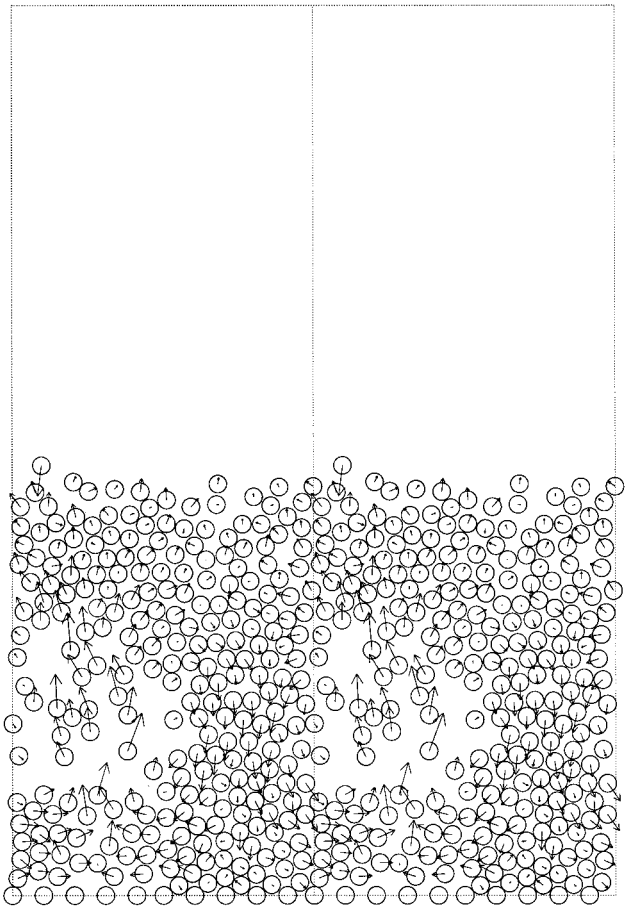

FIG. 8. Convective motion of particles in the bubble at $u^\infty=0.3$ and St=10. Here two periodic images are shown. We can observe the sharp edge of the bubble and the definite convection.

## IV. DISCUSSION

In this section we present two characteristic results of our simulation, which are the height of the center of mass $\overline{H}(\mathrm{St})$ and the diffusion constant $D(u^\infty)$, and then discuss the relation between them. Figure 10 shows $\overline{H}(\mathrm{St})$ for $u^\infty=0.15$, 0.2, 0.3, and 0.5. We see the qualitative change in the transition area in Fig. 1. The clear logarithmical increase of $\overline{H}$ in

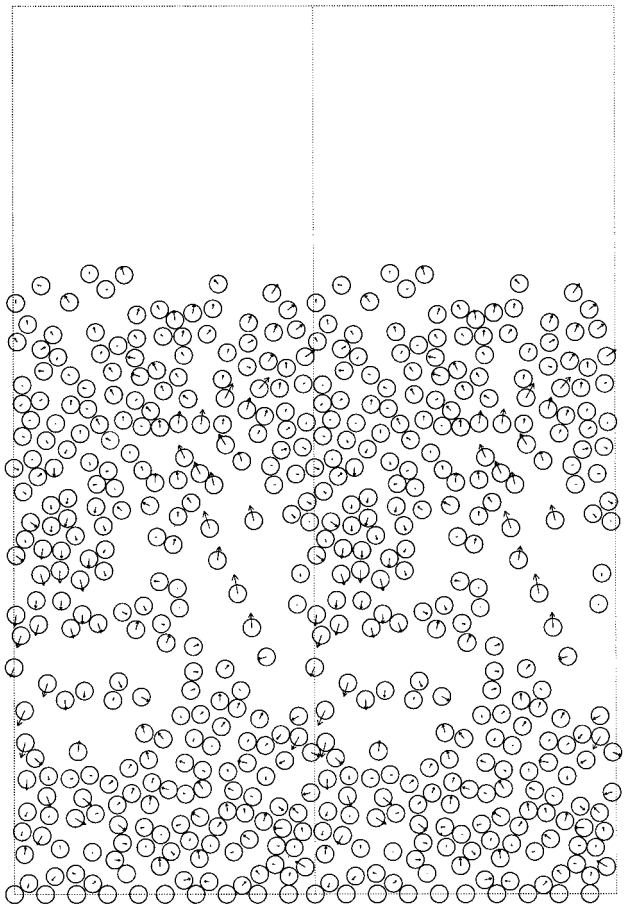

FIG. 9. Convective motion of particles in the bubble at $u^{\infty}=0.3$ and St=100. Here two periodic images are shown. Compared to Fig. 7, we can observe a broader edge of the bubble and weaker convection, where the scale of the velocities are the same.

the bubbling phase is remarkable. We fit the data in Fig. 10 by

$$\overline{H}(\mathrm{St}) = C_H \ln(\mathrm{St}) + D_H, \tag{4.1}$$

where the fitting parameters $C_H$ and $D_H$ depend on $u^{\infty}$. Equation (4.1) can be rewritten as

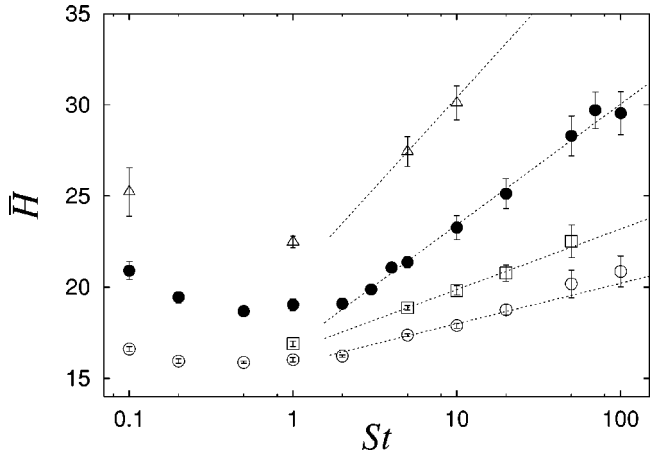


FIG. 10. St dependence of $\overline{H}$ at $u^{\infty}=0.15$ (○), 0.2 (□), 0.3 (●), and 0.5 (△). The fittings by Eq. (4.1) are also shown.

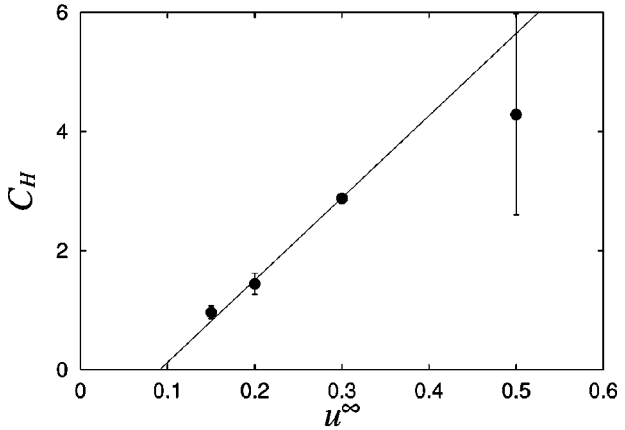


FIG. 11. $u^{\infty}$ dependence of the fitting parameter $C_H$. The solid line shows the fitting by $C_H \propto u^{\infty}-u_c$.

$$\mathrm{St} = \exp\left(\frac{\overline{H}-D_H}{C_H}\right). \tag{4.2}$$

Here $\overline{H}-D_H$ can be understood as the volume expansion $\Delta V$ since $D_H$ is the height at St=1. We show the $u^{\infty}$ dependence of $C_H$ in Fig. 11. From this figure, $C_H$ may be proportional to $u^{\infty}-u_c$. Since St is the characteristic time $\tau$ of the system, we may rewrite Eq. (4.2) as

$$\tau \propto \exp\left(F\frac{\Delta V}{u^{\infty}-u_c}\right), \tag{4.3}$$

where $F$ is a constant. Equation (4.3) suggests that the activation process exists, where $\tau$ is the time to generate the volume expansion $\Delta V$. The importance of an activation process similar to the hole theory for simple liquids [21,22] has been indicated in the compaction process of vibrating beds [23–25]. For dense particle system, it is natural that the viscosity is proportional to the time $\tau$ needed to generate a certain free volume. Therefore, we expect that the effective viscosity $\mu_e$ may be written as

$$\mu_e(u^{\infty}) \propto e^{\varepsilon'/(u^{\infty}-u_c)}, \tag{4.4}$$

where $\varepsilon'$ is a constant. Equation (4.4) is similar to the Vogel-Fulcher law [26,27] in glass-forming liquids. In the experiment of fluidized beds [28], the shear viscosity measured by the modified Stormer viscometer also obeys similar behavior, although it is proposed simply as the Arrhenius function $\exp(\varepsilon'/u^{\infty})$ rather than Eq. (4.4). The result of $\overline{E}(u^{\infty})$ in Fig. 5 suggests that the flow rate $u^{\infty}$ behaves as the effective temperature of the environment as that of the heat bath in equilibrium systems. Therefore, the critical flow rate $u_c$ may correspond to the glass transition temperature.

In Fig. 12 we show $D(u^{\infty})$ in the simulation calculated by

$$D = \frac{1}{2}\frac{1}{N_M}\sum_{\alpha=1}^{N_M} |\tilde{\mathbf{U}}^{\alpha}(\omega=0)|^2, \tag{4.5}$$

where $\tilde{\mathbf{U}}^{\alpha}(\omega)$ is the Fourier transform of $\mathbf{U}^{\alpha}(t)$. We see that $D=0$ for $u^{\infty}<u_c$ and it increases monotonical for $u^{\infty}>u_c$. We also try to fit the data by

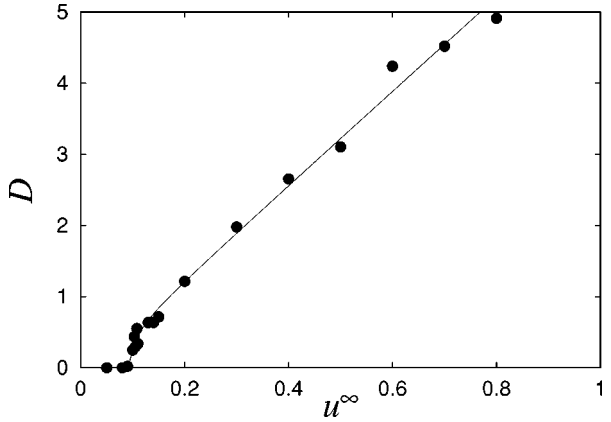


FIG. 12. Flow-rate dependence of the diffusion constant $D$ at St $=10.0$. The fitting by Eq. (4.6) with $\varepsilon=0.113\pm0.017$ is also shown as the solid line.

$$D(u^\infty)\propto u^\infty e^{-\varepsilon/(u^\infty-u_c)}, \tag{4.6}$$

where $\varepsilon$ is a fitting parameter. From Fig. 12, Eq. (4.6) is a good fitting function of the simulation results.

Let us discuss the relation between $\overline{H}(\mathrm{St})$ and $D(u^\infty)$. Equations (4.4) and (4.6) suggest that the diffusion constant $D$ may be related to the viscosity $\mu_e$ as

$$D\propto\frac{u^\infty}{\mu_e}. \tag{4.7}$$

Equation (4.7) suggests that the Einstein relation or the fluctuation-dissipation relation in fluidized beds may exist with the replacement of temperature by the effective temperature $u^\infty$. This statement is interesting because the system is in a highly nonequilibrium state and there is no reason for the existence of the fluctuation-dissipation relation in the sense of linear nonequilibrium statistical mechanics.

Before closing this section, we make the following remarks. Although the transition of fluidization in some experiments seems to be a discontinuous phase transition [29,30], our simulations suggest a continuous phase transition. To remove such a contradiction, we indicate that a recent experiment [31] shows that the continuous transitions are observed in the system with small particles, conventionally called *A* particles of Geldart's classification [32], where the Stokes approximation and our model would be justified. It is also an open problem that at present we cannot reproduce a *homogeneous phase* in our simulation. The reason for the lack of the phase might be the lack of the contact force among particles [30].

## V. CONCLUSIONS

In this paper we have carried out systematic simulations of a fluidized bed with the change of two control parameters $u^\infty$ and St. When the flow rate $u^\infty$ is small, particles are at rest. Above the critical flow rate $u_c$, particles are fluidized. The critical value $u_c$ is independent of St. We have observed two fluidized phases, *the channeling phase* and *the bubbling phase*, where the former changes to the latter as St increases. We have found that the flow rate $u^\infty$ plays the role of the effective temperature. The height of the center of mass $\overline{H}(\mathrm{St})$ in the bubbling phase increase logarithmically with St, which suggests that the effective viscosity obeys the Vogel-Fulcher law (4.4). The diffusion constant $D(u^\infty)$ is well fitted by Eq. (4.6) and this suggests the existence of some kind of fluctuation-dissipation relation in fluidized beds.

## ACKNOWLEDGMENTS

We would like to thank S. Sasa, Y-h. Taguchi, and Ooshida T. for fruitful discussions on the subject of this work. K.I. also thanks M. Doi and J. F. Brady for encouragement and useful comments on this work. This work was partially supported by the Japan Society for the Promotion of Science and a Grant-in-Aid of Ministry of Education of Science and Culture in Japan. Numerical simulations were carried out by the facilities of the Supercomputer Center at the Institute for Solid State of Physics at the University of Tokyo.

## APPENDIX: THE INERTIAL EFFECT OF PARTICLES

Here we discuss the difficulties of the introduction of particle inertia into the Stokes approximation. Let us consider directly the equation of motion of particles with only three mechanisms: the inertial effect of the particles, the hydrodynamic interaction through the fluid under the Stokes approximation, and the gravitational force. Then the equation of motion can be written as

$$\mathrm{St}_0\frac{d\mathbf{U}}{dt}=-\overleftrightarrow{R}\cdot(\mathbf{U}-\mathbf{u}^\infty)-\mathbf{E}_z, \tag{A1}$$

where $\mathrm{St}_0$ is the bare Stokes number defined by

$$\mathrm{St}_0=\frac{mU_0}{6\pi\mu a^2}. \tag{A2}$$

Multiplying $\overleftrightarrow{R}^{-1}$ to Eq. (A1) from the left-hand side, we get

$$\mathrm{St}_0\overleftrightarrow{R}^{-1}\cdot\frac{d}{dt}\mathbf{U}=-\mathbf{U}+\mathbf{V}, \tag{A3}$$

where $\mathbf{V}$ is defined by Eq. (2.3). From the simulation of Eq. (A3), we observe no collision between particles even in the case with large $\mathrm{St}_0$. Particles form a cluster and relative motion among them almost disappears. This situation may be understood by the model

$$\mathrm{St}_0\frac{dU}{dt}=-\frac{1}{2(r-2a)}U. \tag{A4}$$

Here we extract the radial component of the motion between two particles. $r$ denotes the separation between the centers of the pair and $U$ denotes the relative velocity. The resistance $1/2(r-2a)$ reflects the lubrication effect, which diverges at contact $(r\to2a)$. In this case, we need initially the infinite energy to approach the contact point $(r=2a)$ even in the case of large $\mathrm{St}_0$. Thus the model (A4) cannot contain any collision.

Our model (2.1) may be understood as the renormalization of the singularity in the lubrication because we get Eq. (2.1) by multiplying the singularity $\overleftrightarrow{R}$ by the inertial term of Eq. (A3). (Here we note that $\overleftrightarrow{R}$ is dimensionless because it is scaled by $6\pi\mu a$.) Our model behaves reasonably like real fluidized beds where collisions occur so frequently. We can imagine several possible mechanisms preventing the singularity. For example, if there are some dimples on the surface of the particles, they collide before the mean surfaces come in contact. From another point of view we can also say that the continuous description of the fluid in the gap between the particles breaks down when particles approach each other and the gap becomes comparable to the mean free path of the molecules of the fluid [33].

Recently, a model in this context has been presented [34]. To remove the singularity, they introduce a cutoff length, which may correspond to the height of the dimples on the surface or the mean free path of the fluid molecules. Their simulation shows that the results are characterized by a scaled Stokes number that strongly depends on the cutoff length rather than the bare Stokes number. We need to show the renormalization procedure on the particle inertia problem in the Stokes approximation, which we accept *a priori* in Eq. (2.1).


[1] H. M. Jaeger, S. Nagel, and R. P. Behringer, Rev. Mod. Phys. **68**, 1259 (1996).
[2] *Granular Matter—An Interdisciplinary Approach*, edited by A. Mehta (Springer-Verlag, New York, 1993).
[3] H. Hayakawa, H. Nishimori, S. Sasa, and Y-h. Taguchi, Jpn. J. Appl. Phys., Part 1 **34**, 397 (1995).
[4] *Fluidization*, 2nd ed., edited by J. F. Davidson, R. Clift, and D. Harrison (Academic, London, 1985).
[5] D. Gidaspow, *Multiphase Flow and Fluidization* (Academic, London, 1994).
[6] D. A. Drew, Annu. Rev. Fluid Mech. **15**, 261 (1983).
[7] G. K. Batchelor, J. Fluid Mech. **193**, 75 (1988).
[8] S. Sasa and H. Hayakawa, Europhys. Lett. **17**, 685 (1992).
[9] M. F. Göz, Phys. Rev. E **52**, 3697 (1995).
[10] T. S. Komatsu and H. Hayakawa, Phys. Lett. A **183**, 56 (1993).
[11] T. S. Komatsu and S. Sasa, Phys. Rev. E **52**, 5574 (1995).
[12] Y. Tsuji, T. Tanaka, and T. Ishida, Powder Technol. **71**, 239 (1992).
[13] Y. Tsuji, T. Kawaguchi, and T. Tanaka, Powder Technol. **77**, 79 (1993).
[14] T. Tanaka, T. Kawaguchi, and Y. Tsuji, Int. J. Mod. Phys. B **7**, 1889 (1993).
[15] K. Ichiki and H. Hayakawa, Phys. Rev. E **52**, 658 (1995).
[16] K. Ichiki, Ph.D. thesis, Tohoku University, 1996 (in Japanese).
[17] J. F. Brady and G. Bossis, Annu. Rev. Fluid Mech. **20**, 111 (1988).
[18] C. W. J. Beenakker, J. Chem. Phys. **85**, 1581 (1986).
[19] J. F. Brady, R. J. Phillips, J. C. Lester, and G. Bossis, J. Fluid Mech. **195**, 257 (1988).
[20] H. Hayakawa and K. Ichiki, Phys. Rev. E **51**, R3815 (1995).
[21] J. P. Hansen and I. R. McDonald, *Theory of Simple Liquids* (Academic, London, 1986).
[22] J. Frenkel, *Kinetic Theory of Liquids* (Oxford University Press, London, 1946).
[23] H. Hayakawa and D. C. Hong, Phys. Rev. Lett. **78**, 2764 (1997).
[24] E. Caglioti, V. Loreto, H. J. Herrmann, and M. Nicodemi, Phys. Rev. Lett. **79**, 1575 (1997).
[25] T. Boutreux and P. G. de Gennes, Physica A **244**, 59 (1997).
[26] H. Vogel, Phys. Z. **22**, 645 (1921).
[27] G. S. Fulcher, J. Am. Ceram. Soc. **8**, 339 (1925).
[28] J. Furukawa and T. Ohmae, Ind. Eng. Chem. **50**, 821 (1958).
[29] A. Lippert, Chem. Ind. Tech. **38**, 350 (1966).
[30] S. C. Tsinontides and R. Jackson, J. Fluid Mech. **255**, 237 (1993).
[31] G. D. Cody, D. J. Goldfarb, J. G. V. Storch, and A. N. Norris, Powder Technol. **87**, 211 (1996).
[32] D. Geldart, Powder Technol. **7**, 285 (1973).
[33] R. R. Sundararajakumar and D. L. Koch, J. Fluid Mech. **313**, 283 (1996).
[34] A. S. Sangani, G. Mo, H.-K. Tsao, and D. L. Koch, J. Fluid Mech. **313**, 309 (1996).